frontiers | Frontiers in Earth Science

TYPE Original Research
PUBLISHED 12 October 2023
DOI 10.3389/feart.2023.1259178

OPEN ACCESS

EDITED BY
Xijun Liu,
Guilin University of Technology, China

REVIEWED BY
Meng Wang,
Chang'an University, China
Jinning Zhang,
China University of Petroleum, Beijing, China

*CORRESPONDENCE
Di Li,
lidi@cugb.edu.cn

RECEIVED 15 July 2023
ACCEPTED 16 August 2023
PUBLISHED 12 October 2023

CITATION
Zhen Y, Xu X, He D, Li X and Li D (2023), Discovery of the large-scale thrust nappe and its geological significance in the southwestern Santanghu fold–thrust belt, NW China.
Front. Earth Sci. 11:1259178.
doi: 10.3389/feart.2023.1259178

Discovery of the large-scale thrust nappe and its geological significance in the southwestern Santanghu fold–thrust belt, NW China

Yu Zhen[1,2], Xiongfei Xu[3], Dengfa He[1,2], Xinning Li[3] and Di Li[1,2]*

[1]School of Energy Resources, China University of Geosciences, Beijing, China, [2]Key Laboratory of Marine Reservoir Evolution and Hydrocarbon Enrichment Mechanism, Ministry of Education, Beijing, China, [3]Research Institute of Exploration and Development, Tuha Oilfield Company, PetroChina, Hami, China

Studying the structural evolution of the piedmont fold and thrust belt is one of the most important methods to interpret the mechanism of intracontinental collision orogeny. In this study, we have discovered a long-distance large-scale thrust nappe with a width of approximately 20 km in the southwestern margin of the Santanghu Basin, which provides a good evidence for studying the Mesozoic–Cenozoic tectonic evolution mechanism of Moqinwula Mountain. Using the electromagnetic and high-resolution seismic profiles, we have determined that the hanging wall of the nappe is composed of the pre-growth strata of the Carboniferous–Middle Jurassic period and the syntectonic strata of the Cretaceous–Quaternary period. The nappe is subjected to two branch faults of the Baiyishan thrust, forming a breakthrough fault-propagation fold and a fault-bend fold along the detachment layer of the Haerjiawu Formation, and a large monoclinic is formed by the basement structural wedge near the mountain root. The growth strata and unconformity structure record that the fold–thrust belt has experienced five episodes of thrusting from the Late Triassic to Quaternary period. Based on sequential restoration and forward modeling, we propose that the southwestern margin of the Santanghu Basin has been shortened by at least 55 km, especially in the Late Jurassic and Late Cretaceous. Our results provide an excellent example for studying the mechanism of the transition from Yanshanian transpression to Himalayan thrust compression in the Eastern Tianshan region.

KEYWORDS

Eastern Tianshan, southwestern Santanghu Basin, fold-thrust belt, intracontinental orogeny, thrust nappe

1 Introduction

The piedmont Basin records the stratigraphic and structural information on deformation during the orogenic process (e.g., DeCelles, 2011; Jiang and Li, 2014). The deformation propagation from the orogenic belt to the basin is an important process to accommodate with crustal shortening and erosion (Davis et al., 1983; Suppe and Medwedeff, 1990). In the intracontinental orogenic deformation system, the front edge of the orogenic wedge is deformed into a series of fault-related folds and related thrust basins (e.g., Tesón et al., 2010; Alania et al., 2022; Yu et al., 2023). The syntectonic sedimentation of the thrust basin provides the deformation history record of related structures, which is one of the

important indication to judge the shortening and uplift time of the orogenic belt (Tesón and Teixell, 2008; Sun and Zhang, 2009; Izquierdo-Llavall et al., 2018).

The Tianshan Orogenic Belt (TOB) stretches for more than 2,500 km and is located at the southernmost tip of the Central Asian Orogenic Belt (CAOB) (Figure 1A), which is one of the most famous intracontinental orogenic belts in the world (Sengör et al., 1993; Windley et al., 2007). The TOB was initially formed by the accretion of continental blocks from the Neoproterozoic to Permian period and then underwent multi-episodic uplift and orogeny from the Mesozoic to Cenozoic period (Charvet et al., 2007; Jolivet et al., 2013). The Moqinwula Mountain is located in the easternmost part of the TOB in China, which has formed a large-scale fold–thrust belt (FTB) in the southern margin of the Santanghu Basin (Figure 1B). However, because the piedmont zone of Moqinwula Mountain is covered by the Quaternary strata, there is a lack of Mesozoic–Cenozoic sediments and tectonic deformation records on the surface, which makes it difficult to analyze the intracontinental deformation mechanism of the orogenic belt. Although previous studies on the Mesozoic–Cenozoic tectonic history of Moqinwula Mountain have established the deformation mechanism of multi-stage episodic uplift and exhumation of the orogenic belt, these studies mainly relied on the geothermal thermochronology method at the outcrop scale and did not establish a quantitative continuous evolution process (Gillespie et al., 2017; Chen et al., 2020a; He et al., 2022). In contrast, high-resolution seismic profiles of piedmont belts can reveal continuous records of the propagation and deformation of orogenic belts to basins, which is one of the important methods to analyze the evolution of orogenic belts and basins (Allen and Allen, 2013).

Therefore, we used the digital elevation model, boreholes, high-resolution electromagnetic profiles, and seismic data on the Moqinwula Mountain piedmont zone to characterize the geometry of the fold–thrust belt in the southern margin of the Santanghu Basin. Based on the growth strata and unconformity exposed by seismic profiles, combined with the low-temperature thermochronological data reported by predecessors, we established the spatio-temporal framework and tectonic kinematics mechanism of regional tectonic evolution. Using these results, we discussed the mechanism of multi-stage episodic deformation of the large-scale nappe in the piedmont zone under the intracontinental orogenic system and provided an excellent example for studying the Mesozoic–Cenozoic tectonic evolution in the Eastern Tianshan region.

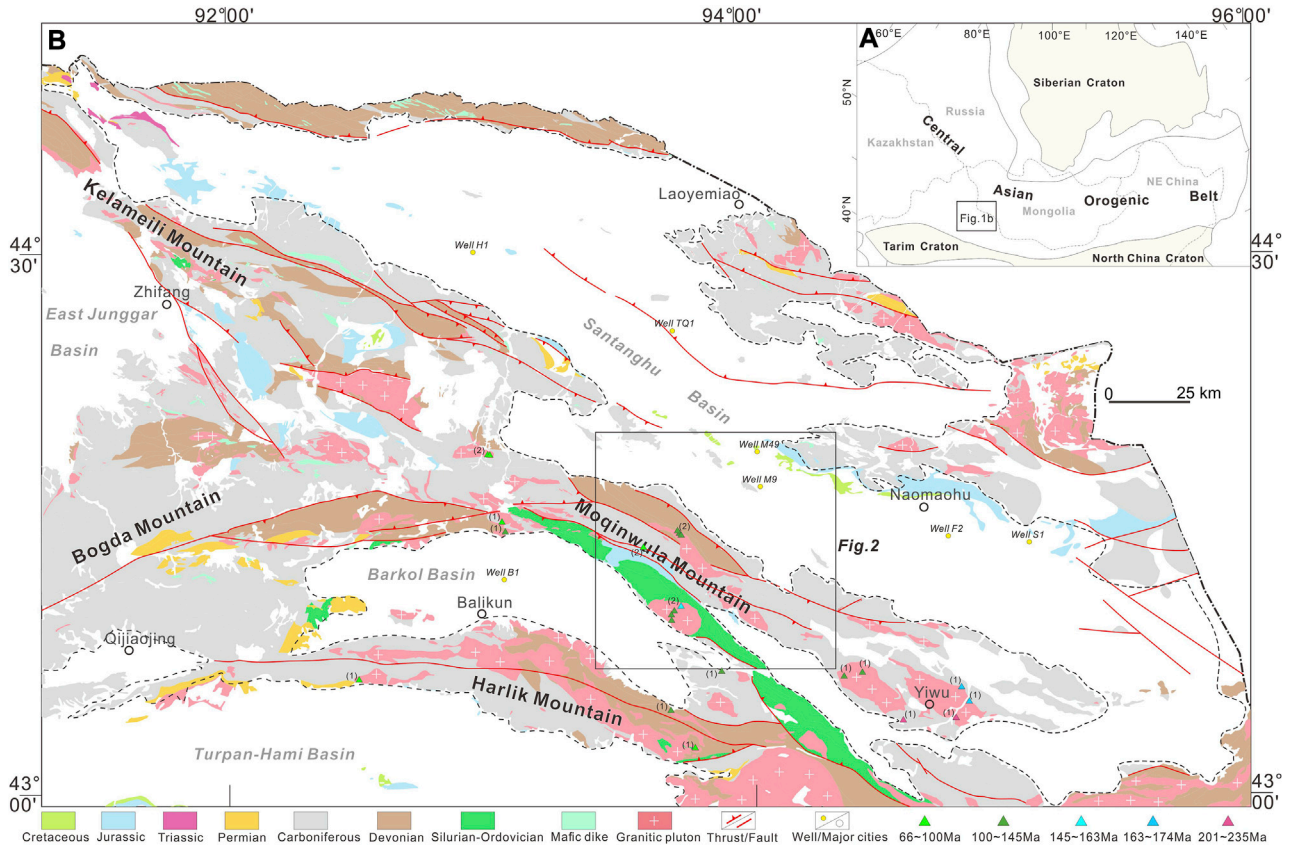

FIGURE 1
(A) Tectonic relationship of the Tianshan Orogenic Belt (TOB) to the Central Asian Orogenic Belt (modified after Sengör et al., 1993; Windley et al., 2007). **(B)** Simplified geologic map of the Eastern Tianshan region (modified after BGMRXUAR, 1966). The apatite fission track age data are from (1) Gillespie et al., 2017 and (2) Chen et al., 2020a.

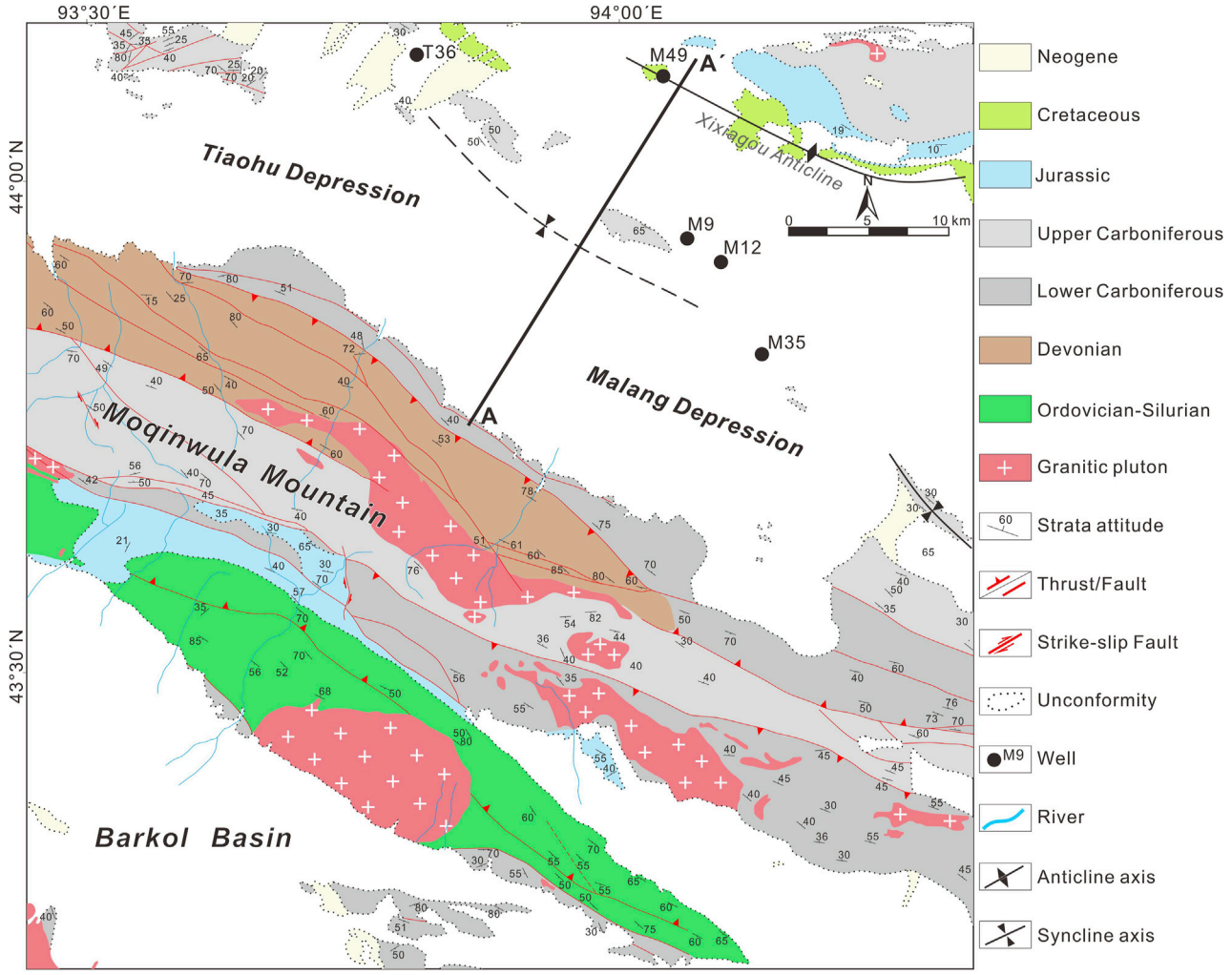

FIGURE 2
Geological map of the southwestern Santanghu fold–thrust belt (modified after BGMRXUAR, 1966), showing the distribution of the main structures, the geological units exposed on the surface, and the location of the cross section.

2 Geologic setting

2.1 Tectonic setting

The Santanghu Basin is located on the accretion zone of the southern margin of the Siberian Plate, and it is also a collision joint with the Kazakhstan Plate (Ma et al., 1993; Shu et al., 2001; Xiao et al., 2004). It is a micro-block between the northwest Altai and the Kalamaili suture zones, which is superimposed on the Paleozoic fold orogenic system (Xiao et al., 2004; Zhou et al., 2004; Chen et al., 2009). The Santanghu Basin is a NW-trending strip-shaped contour, which is approximately 500 km long and 40–70 km wide (Figure 1B). Affected by the thrust tectonic activities of the northern Altai Mountains and the southern Moqinwula Mountains, the tectonic framework of the basin in the northwest-southeast direction was formed. The fold–thrust belt in the southwestern margin extends from the front of the Moqinwula Mountains to the center of the basin, and the extrusion thrust front belt exposes the Upper Carboniferous on the surface (Figure 2), forming a northwestward arc belt extending 60–70 km on the map (Figure 1B).

In the Late Paleozoic, northern Xinjiang was influenced and restricted by many subduction suture zones, such as Kalamaili and Altai, showing the ancient tectonic environment of the multi-island residual sea basin (Xiao et al., 2009). In particular, the divergent double subduction suture zones of Kalamaili and Altai controlled the subduction, reduction, and closure of residual basins in the basin area (Wang et al., 2019; Li et al., 2020). In the Early Carboniferous, the Santanghu Basin was a part of the residual sea basin of the East Junggar island arc. In the Late Carboniferous, the collision between the Kazakhstan and Siberian plates resulted in the closure of the oceanic basin (Huang et al., 2018). The Permian was a post-collisional relaxation transition period, and the Late Permian–Early Triassic was transformed into a compressional uplift (Zhao et al., 2020). The Jurassic–Paleogene Basin entered the stage of compression

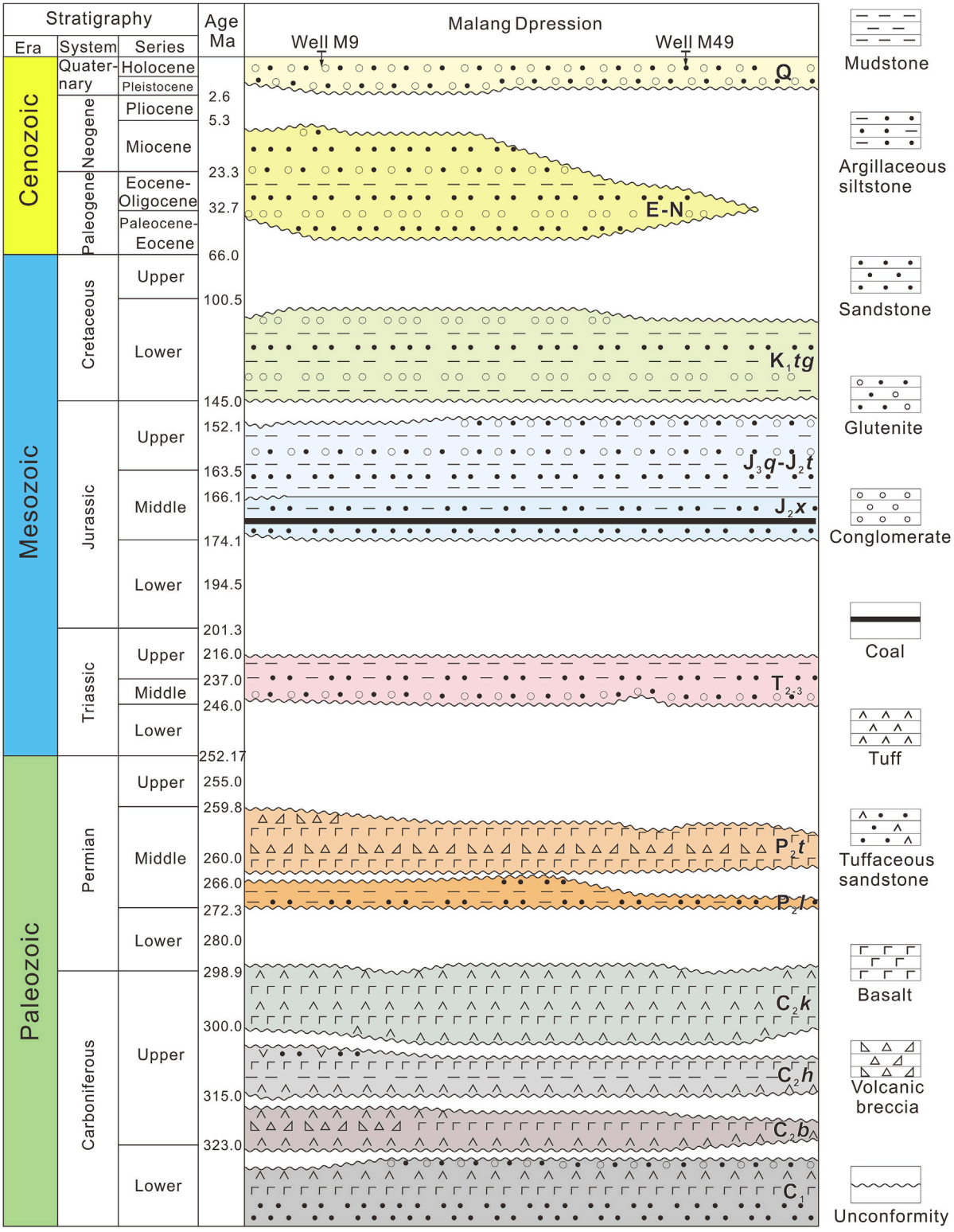

FIGURE 3
Chronostratigraphic column shows the main stratigraphic units and major unconformities in the study region (data from the drilling wells M49 and M9). The profile location is shown in Figure 2.

depression. Under the influence of the NS trending compression tectonic activity in the Yanshanian movement, the basin margin developed a strike–slip fault system along the northwest direction (Lu et al., 2012; Chen et al., 2020b). Since the Neogene, the basin has entered the stage of transformation, forming the current regional structure.

2.2 Stratigraphy

The Carboniferous strata include the Donggulubasitao, Jiangbasitao, Batamayineishan, Haerjiawu, and Kalagang Formations. It belongs to the marine and marine–continental sedimentary environment, and specifically develops volcanic rocks and clastic rocks with carbonaceous shale and coal seams (Figure 3). The Lower Permian and Upper Permian are missing in the region. The Middle Permian strata include the Lucaogou and Tiaohu Formations. The Lucaogou Formation is widely distributed in the Tiaohu and the Malang Depression, and the lithology is mainly tuffaceous glutenite, sandstone, and muddy limestone. Basalt is developed at the bottom of the Tiaohu Formation, fluvial–swamp clastic rock is developed in the middle, and andesite–basalt is developed at the top. The Triassic strata are a set of fluvial-lacustrine facies deposits, which is mainly composed of glutenite, argillaceous siltstone, and mudstone. The Lower Jurassic is absent in the Malang Depression (Si et al., 2015), and the Middle–Upper Jurassic is mainly developed. The Middle Jurassic includes the Xishanyao and Toutunhe Formations. The Xishanyao Formation is characterized by braided river and meandering river deposits, and is sandwiched with multiple layers of coal. The Toutunhe Formation–Upper Jurassic Qigu Formation comprises coarse clastic deposits of fluvial facies and alluvial fan facies. The Cretaceous strata only develops the Tugulu Group, which is a fluvial facies coarse clastic rock deposit. The lithology is mainly conglomerate, sandstone, and mudstone, which is in unconformity with the underlying Jurassic. The Paleogene–Neogene strata are dominated by fluvial facies and alluvial fan deposits. The lithology is interbedded with sand, conglomerate, and mudstone, which is in unconformity with the Cretaceous strata. The Quaternary is widely developed in the basin. The lithology is mainly yellow gravelly clay and glutenite, which is in unconformity with the underlying strata.

3 Data and methods

In this study, we mainly used a high-resolution prestack depth migration seismic profile and an electromagnetic profile in the southwestern Santanghu Basin, which were collected and processed by Tuha Oilfield Company of China National Petroleum Corporation from 2021 to 2022, to interpret the structure of the piedmont zone. We calibrated the Carboniferous–Quaternary strata in the seismic profile by using the key drilling wells (M9 and M49) in the Malang Depression. With the support of logging and lithology data, we obtained the synthetic seismic records and identified the following key marker layers (Figure 4): the sandstone at the bottom of the Lucaogou Formation is in unconformity contact with the basalt of the underlying Kalagang Formation. Glutenite at the bottom of the Middle Triassic Xiaoquangou Group is in unconformity contact with basalt at the top of the Middle Permian Tiaohu Formation. The coal seams developed in the Lower Jurassic Xishanyao Formation are characterized by high GR and high RT on logging curves, and show strong amplitude and good continuity in synthetic seismic records. In addition, we traced the strata inside the Heidrun nappe by means of seismic wave group characteristics, thickness comparison, and unconformity identification. The structural characteristics of the piedmont zone are mainly based on the 1: 200000 geological mapping of the Moqinwula Mountain area to constrain the faults and stratigraphic occurrences exposed on the surface (BGMRXUAR, 1966). Under the constraint of regional unconformity in the piedmont zone, we determined the main period of structural deformation. Based on the principle of layer length and thickness conservation, we used the 2D MOVE software developed by Petroleum Experts (Petex) to balance and restore the kinematics of the cross section.

4 Result

4.1 Structural features of the southwestern Santanghu fold-thrust belt

The electromagnetic profile reveals that there is a high-resistivity area $10^{(2.5-4)}(\Omega \times m)$ with a length of approximately 19 km higher than the depth of 3 km in the piedmont zone (Figure 5). Combined with the outcrop of Carboniferous exposed on the map (Figure 2), we believe that this tectonic belt is the result of long-distance thrusting of Carboniferous and overlying strata. A low-resistivity zone ($10^{(1.4-3)}$ $\Omega \times m$) with a thickness of approximately 2–3 km is preserved under the thrust nappe, which is similar to the resistivity value of the Carboniferous Kalagang Formation–Permian Tiaohu Formation in the Malang Depression. The lithology combination of volcanic rocks and sedimentary rocks is developed in the Carboniferous of Malang Depression (Figure 4), and the resistivity of basement Carboniferous is relatively large ($10^{(3.5-5)}$ $\Omega \times m$), which reveals an obvious uplift–depression structure controlled by faults. In contrast, the resistivity of sedimentary cover in the footwall of the thrust nappe is relatively small ($10^{(1.5-2.5)}$ $\Omega \times m$), and the degree of extrusion deformation is weak. Lithology and logging data from drilling wells M9 and M49 in the Malang Depression show that the resistivity of the Triassic–Quaternary clastic sedimentary rocks is low, while the overall resistivity of the Carboniferous–Middle Permian is high due to the increase in the proportion of volcanic rocks (e.g., basalt and andesite), and the local low resistivity layer usually indicates the detachment layer.

The high-resolution 2D seismic profile shows that the Heidun nappe cuts the Carboniferous–Permian by two Baiyishan branch faults developed along the detachment layer of the Haerjiawu Formation (Figure 6). The detachment fault flat at the bottom of the root zone of the nappe is close to horizontal, and the dip angle of the lower thrust slope is approximately 28–44°. According to the monoclinic syncline axis, the endpoint of the structural wedge is limited. The Carboniferous–Jurassic deformation on the hanging wall of the back-thrust fault is consistent with the fault dip angle. The Kalagang Formation above the wedge endpoint is locally thickened and thinned upward, indicating the internal pre-existing normal fault. The front of the wedge endpoint is composed of two branch faults: F1 and F2 of the Baiyishan fault (Figure 6). The top end of the F1 fault terminates below the Cretaceous, and we identify two sets of dip domains (16° and 40°). The folds formed on the hanging wall are characterized by a long back limb (3–4 km) and a short front limb (1 km). The Carboniferous–Permian fault distance is

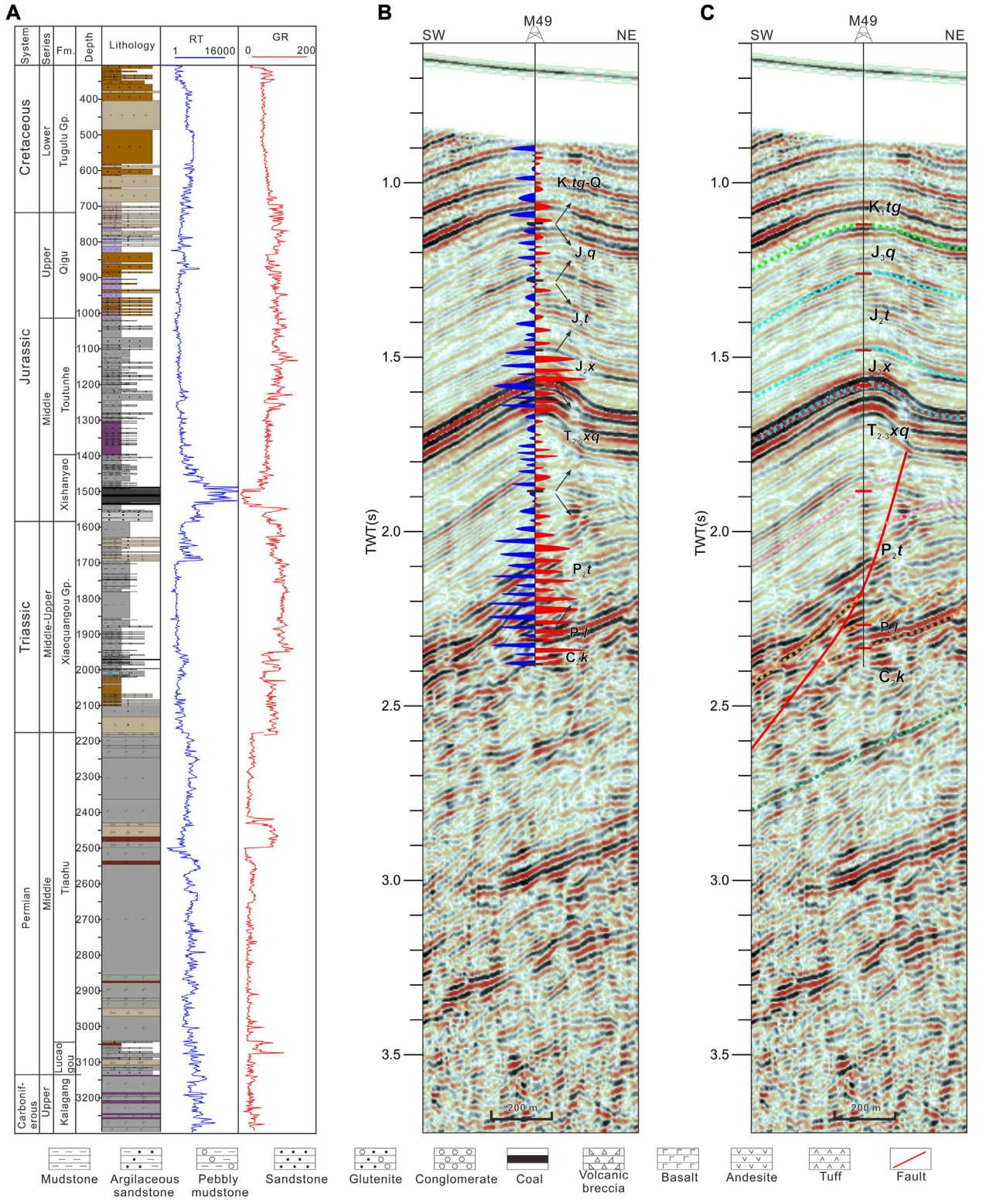

FIGURE 4
(A) Formation lithologic features of drilling well M49 in Malang depression, Santanghu basin. **(B)** Synthetic seismic record of well M49 and its geological interpretation. **(C)** Comprehensive seismic interpretation of well M49.

gradually reduced, showing the characteristics of breakthrough fault-propagation folds. The detachment fault flat of the F2 fault is connected with the F1 fault, and two sets of dip angles (12° and 46°) are developed to the front end. The footwall ramp and the hanging wall fault flat area are relatively intact, and the hanging wall ramp is eroded by long-distance nappe uplift.

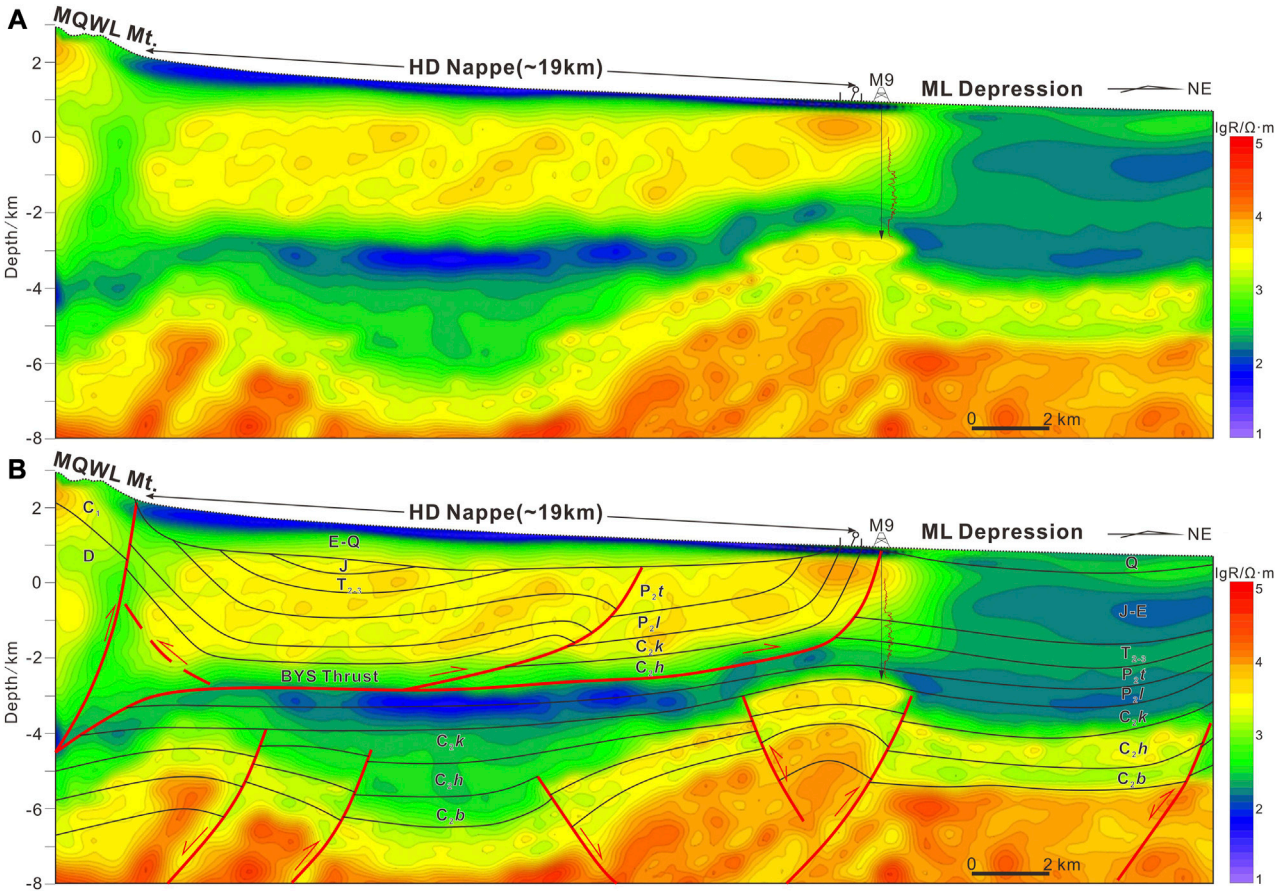

FIGURE 5
Regional electromagnetic section cutting across the Heidrun thrust nappe, showing an uncoordinated hierarchical deformation system (see location in Figure 2). **(A)** Regional electromagnetic section. **(B)** Geological interpretation of electromagnetic section.

The footwall of the Heidrun nappe is dominated by low-relief folds, and two south-dipping high-angle thrust faults are developed in the basement–Carboniferous strata (Figure 6). The top point of the fault near the piedmont zone terminates in the Middle Permian. The length ratio of the back limb (3.55 km) to the front limb (0.62 km) is close to 6: 1, which has the characteristics of a fault-propagation fold. We noticed that the displacement of the faults in the Carboniferous Batamayineishan Formation–Kalagang Formation changed from bottom to top (Figure 6), which were −0.46 km, −0.31 km, and 0.15 km, respectively, indicating the phenomenon of reactivation and inversion of extensional faults. The basement faults in the distal domain show similar characteristics. In particular, the Upper Carboniferous Haerjiawu Formation shows the characteristics of the deposition during the active period of the fault, that is, the thinning from the upper wall of the fault to the side away from the fault, accompanied by overlap unconformity. The detachment folds of the Middle Permian–Paleogene are superimposed above the basement faults in the distal domain, and the overall deformation relief is low. The Xixiagou anticline on the north side of the cross section is interpreted as an asymmetric anticline formed along the detachment thrust of the Carboniferous Kalagang Formation (Figure 8). The top point of the fault is limited to the Middle Permian Tiaohu Formation through the syncline axis, and the basal detachment is connected to the endpoint of the basement fault, indicating the reactivation of the basement fault. The fault consists of two dip domains (27° and 54°), and the fault displacement is approximately 1.4 km.

4.2 Growth strata and unconformities in the southwestern Santanghu Basin

The seismic profile shows that the hanging wall of the Heidrun nappe presents the structure of the piggy-back basin. The internal syntectonic growth strata include the Cretaceous–Quaternary strata, which record the three stages of growth unconformity (Figure 7). The Lower Cretaceous is relatively preserved in the syncline and overlying unconformity above the underlying strata, and the top is cut off by the Paleogene. We noted that the fold structure of the Cretaceous growth strata was spatially consistent with the synclinal axis of the Baiyishan fault and showed a typical growth triangle structure in the front edge of the nappe, with a dip angle of approximately 22° (Figure 7). The truncated unconformity surface of the Paleogene and underlying strata is folded at the root and front of the nappe. The Paleogene–Neogene strata

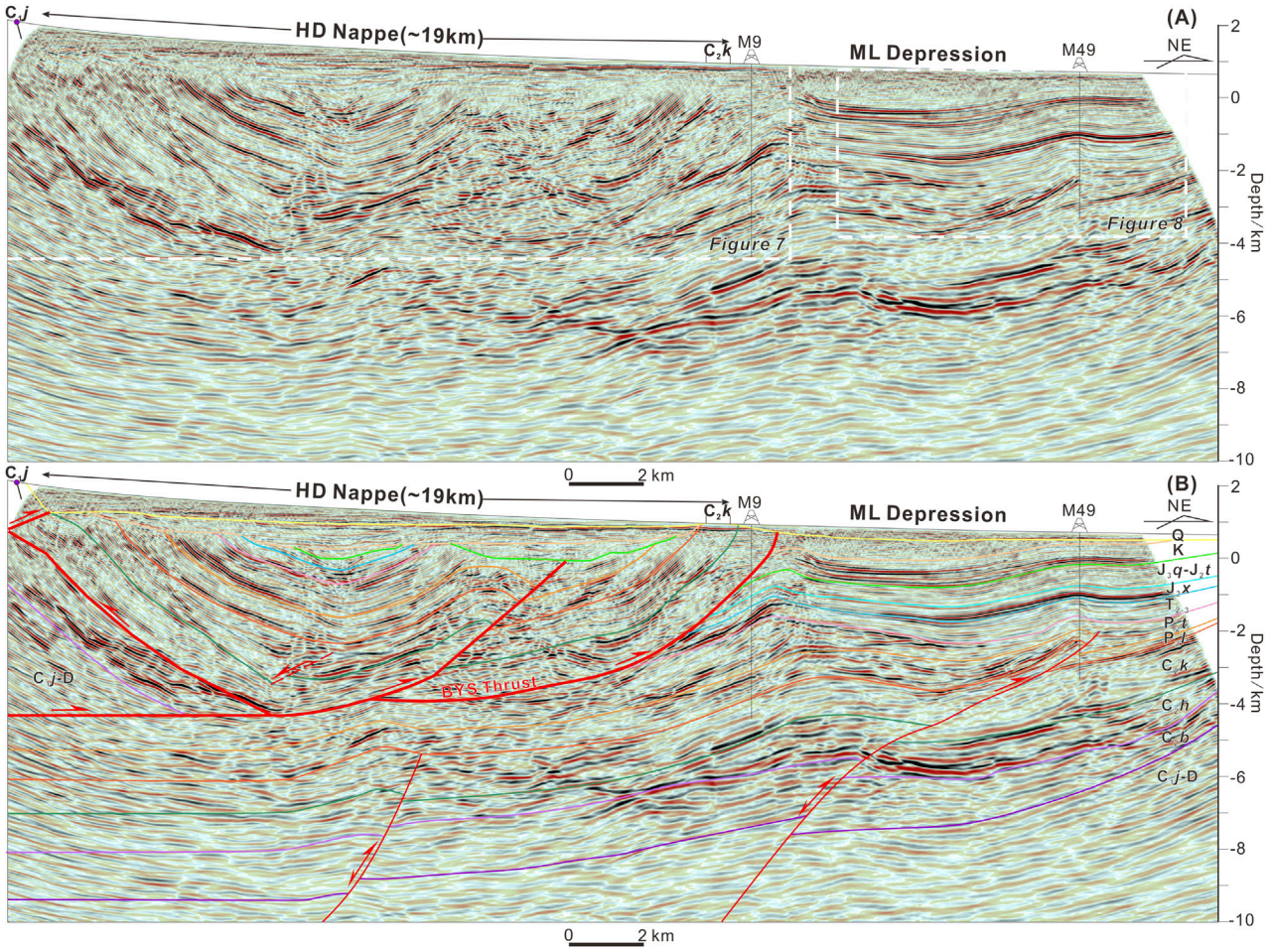

FIGURE 6
Comprehensive seismic imaging profile A-A′ and its geological interpretations. **(A)** Seismic profile cutting across the Heidun thrust nappe. **(B)** Geological interpretation result. The location is shown in Figure 2. C_2b = Carboniferous Batamayineishan Formation (Fm.); C_2h = Carboniferous Haerjiawu Formation; C_2k = Carboniferous Kalagang Formation; P_2l = Middle Permian Lucaogou Formation; P_2t = Middle Permian Tiaohu Formation; $T_{2\text{-}3}$ = Middle–Upper Triassic Xiaoquangou Group; J_2x = Middle Jurassic Xishanyao Formation; J_2t = Middle Jurassic Toutunhe Formation; J_3q = Upper Jurassic Qigu Formation; K = Cretaceous; E = Paleogene; N = Neogene; Q = Quaternary.

overlap on the underlying strata along the unconformity surface, and the internal deformation is relatively weak. The Quaternary is affected by faults in the Moqinwula Mountains to form folds, and there is almost no obvious deformation above the nappe, showing a wedge-shaped northward overlap thinning, indicating the process of flexural adjustment due to orogenic belt uplift during this period.

The Xixiagou anticline is characterized by an asymmetric structure of fault-propagation folds controlled by south-dipping faults (Figure 8). On the map, the Xixiagou anticline is closer to the piedmont deformation zone in the northern part of the Santanghu Basin, recording the complete tectonic deformation history of the basin (Figure 2). The Middle Permian of the Xixiagou anticline gradually uplifts and thins to the north, and the internal development of overlap and truncation unconformity indicates that it is limited by the paleogeomorphology at that time. The Middle Permian of the Xixiagou anticline is cut by the Triassic, and the Middle Triassic overlapped from the limb to the core, indicating the tectonic activity between the Late Permian and the Late Triassic. The Lower Jurassic is missing in Malang Depression, and the Middle Jurassic parallel unconformity covers the Middle Triassic. The Middle–Upper Jurassic shows that it thinned from northeast to southwest, and the core of the anticline is partially cut off by the Cretaceous, indicating that the paleotopography of the southern side of the Xixiagou anticline in the late Middle Jurassic was higher, and the paleotopography of the Late Jurassic gradually increased to the north. The top of the Lower Cretaceous is cut off by the Paleogene in the core of the anticline, and the thickness of the strata gradually thinned northward. The erosion of the Paleogene–Neogene increased in the northwest direction, showing a syntectonic growth stratigraphic structure (Figure 8).

4.3 Sequential restoration of the cross section

We took the north limb of the Xixiagou anticline as the pin line and used the fault parallel flow and line length recovery technology to restore the cross section in sequence. According to the growth

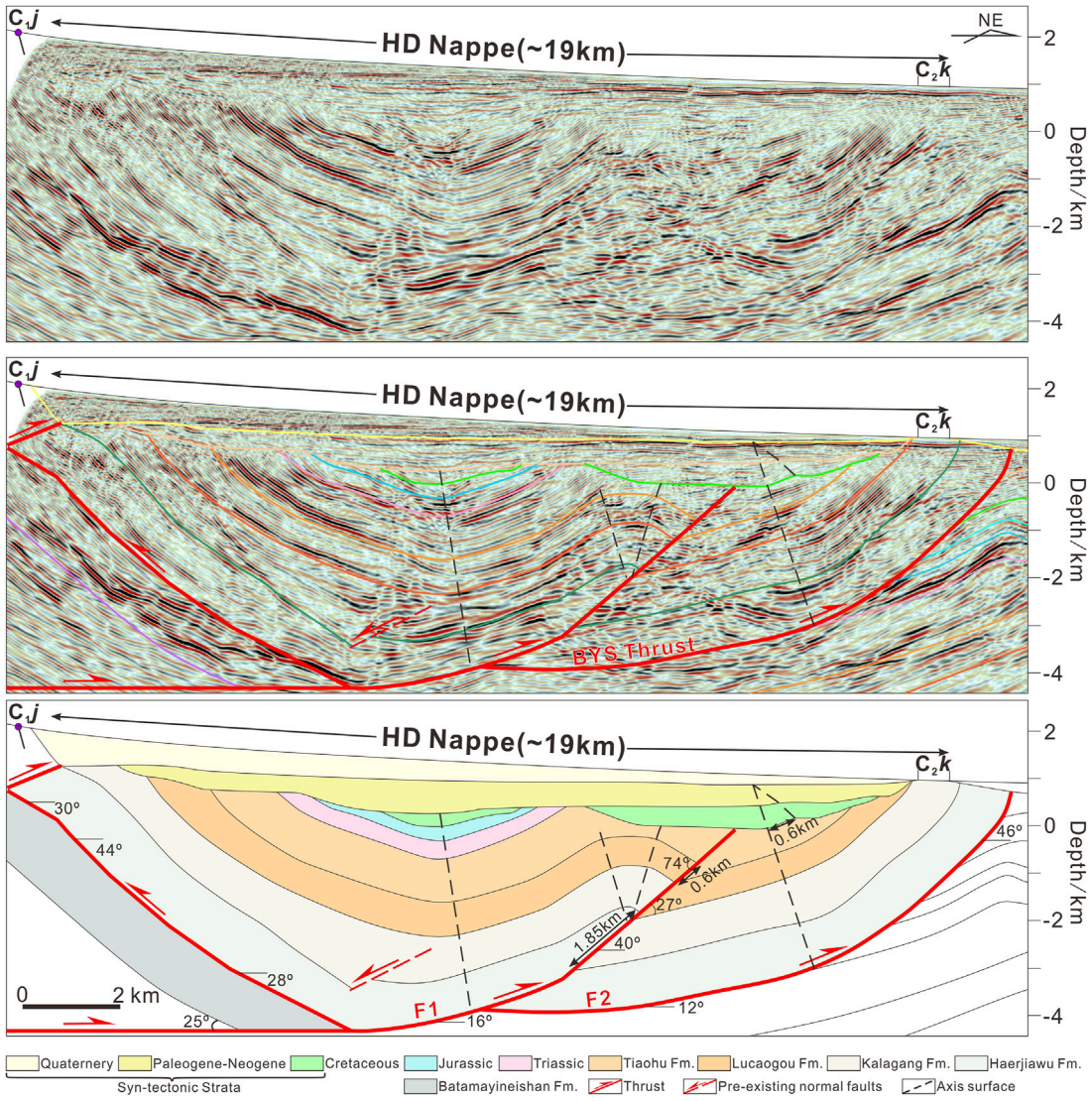

FIGURE 7
Seismic reflection profile and related structural interpretation of the Heidrun thrust nappe show the main faults and stratigraphic structure.

strata and unconformity revealed by the Heidrun nappe and the Xixiagou anticline, we divided the study area into five key compression deformation periods: Late Triassic, Late Jurassic, Late Cretaceous, Paleogene–Neogene, and Quaternary. During the multi-stage compression process, the strata at the top of the nappe are denuded. Therefore, in the restoration process of the cross section, we assumed the erosion strata through the structure and displacement of the fault (Figure 9).

4.3.1 Late Triassic

Influenced by the Indosinian movement, the fold–thrust belt in northern Moqinwula Mountain was pushed forward to the Santanghu Basin by compression. The deformation developed a low-relief fault-propagation fold along the detachment layer of the Carboniferous Haerjiawu Formation. The end of the F1 fault propagated to the top of the Permian Lucaogou Formation, with a fault displacement of approximately 1.09 km (Figure 9B).

4.3.2 Late Jurassic

Affected by the Yanshanian movement, the deformation of the Late Jurassic piedmont zone was further intensified (Figure 9C). The pre-existing F1 fault was reactivated, and the fault endpoint propagated upward, causing fold deformation of the shallower strata. The compression activity resulted in the development of a fault-bend fold with multi-fault ramp-flat on the detachment layer of the Haerjiawu Formation. The hanging wall continued to slide along the detachment layer of the top Middle Permian Tiaohu Formation, entered the deformation of the fold crestal broadening period, and formed the blind thrust fault F2 at the front. We reconstructed the axial of the large-scale nappe eroded by the Carboniferous–Jurassic transition along the fault and estimated the displacement of approximately 35.06 km based on the layer length and fault displacement. During the same period, the pre-existing normal faults of the Carboniferous in the Malang Depression were reactivated, and the upward

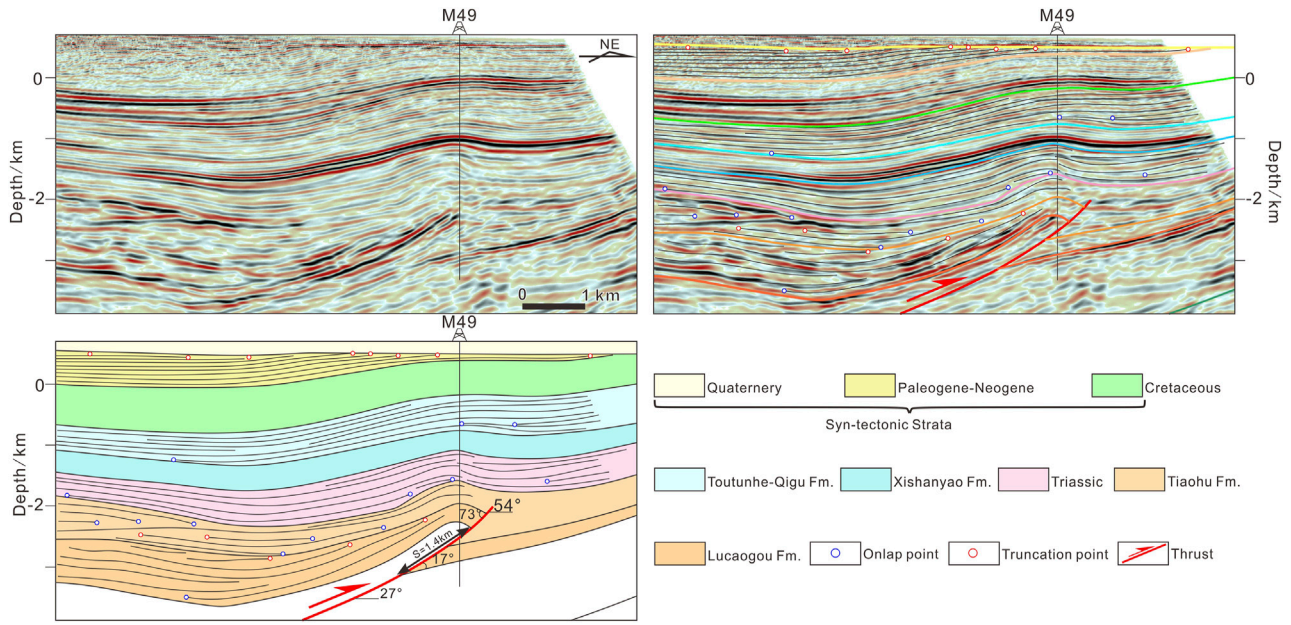

FIGURE 8
Seismic reflection profile and related structural interpretation of the Xixiagou anticline show the main growth unconformities. Structural interpretations show the onlap points (blue points) and truncation points (red points).

propagation of the fault endpoint terminated in the Middle Permian Tiaohu Formation, forming a low-relief fault-propagation fold, with a fault displacement of approximately 1.32 km.

4.3.3 Late Cretaceous

In the Early Cretaceous, the basin and its periphery were in a relatively stable tectonic environment. In the Late Cretaceous, influenced by the two-stage compressional tectonic activities of the Yanshanian movement, a large-scale structural wedge was developed in the basement of the basin margin, resulting in the passive uplift of the Carboniferous–Cretaceous on the southwest side of the Heidrun nappe and the overall northward tilt (Figure 9D). According to the dip angle, layer length, and formation thickness of the front limb, we estimated that the fault displacement was approximately 18.21 km. In addition, the end of the structural wedge continued to break northward along the sliding layer of the Haerjiawu Formation on the roof, resulting in a slip of 1.2 km on the F2 fault.

4.3.4 Paleogene–Neogene

In the late Yanshanian movement, the tectonic activity in the basin margin was weak, and the displacement of the tectonic wedge fault was approximately 1.43 km, which caused the vertical uplift of the structural wedge, and the displacement of the wedge tip to the north was approximately 0.6 km. Due to the orogenic activity of Moqinwula Mountain, the basin deposits dip gently to the southwest (Figure 9E).

4.3.5 Quaternary

During the Himalayan movement, the basin was mainly adjusted and reactivated. The boundary fault activity of the Carboniferous in Moqinwula Mountain caused the Quaternary forced folding (Figures 2, 6), while the internal shortening of the basin could be neglected (Figure 9F).

5 Discussion

5.1 Formation mechanism of the large-scale thrust nappe

The newest electromagnetic profile and high-resolution seismic profile show the deformation structure of the Heidrun nappe (Figures 5, 6), which is quite different from the previous structures formed by large basement-involved faults established in the southern piedmont zone of the Santanghu Basin (Sun et al., 2001; Wu et al., 2011). Previous studies have shown that there are multiple solutions to the activity intensity and sequence of faults in the structural analysis of the piggy-back basin (Alania et al., 2017). In particular, the deformation of the pre-growth strata lacking syntectonic deposits requires the establishment of a reasonable model for structural numerical simulation.

The cross section shows that the Heidrun nappe root zone develops the forward thrust faults and back-thrust faults that cut the Devonian–Carboniferous to form a structural wedge. The detachment layer of the Carboniferous Haerjiawu Formation develops two branch faults along the fault flat to the north, forming a relatively breakthrough fault-propagation fold and a fault-bend fold (Figure 7). The results of the sequential restoration section show that the shortening of the fold–thrust belt reaches 55.79 km, of which 18.21 km is attributed to the basement structural wedge (Figure 9). The forward modeling

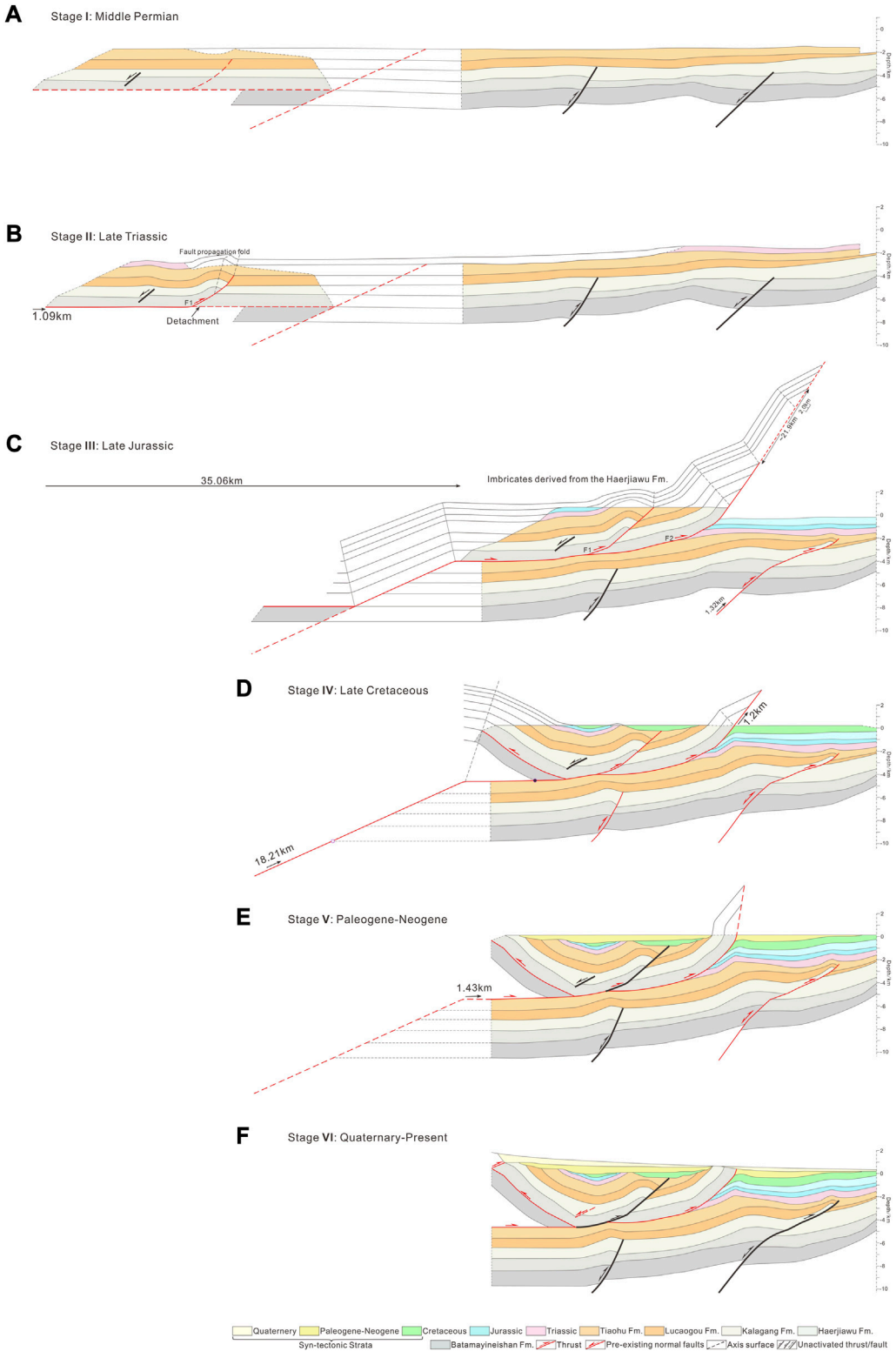

FIGURE 9
Sequential evolution of the Heidrun thrust nappe and adjoining Malang Depression from Late Triassic to Quaternary, based on the restoration of the cross section. **(A)** Restored cross-section during Middle Permian. **(B)** Deformation during Late Triassic. **(C)** Deformation during Late Jurassic. **(D)** Deformation during Late Cretaceous. **(E)** Deformation during Paleogene-Neogene. **(F)** Deformation during Quaternary-Present.

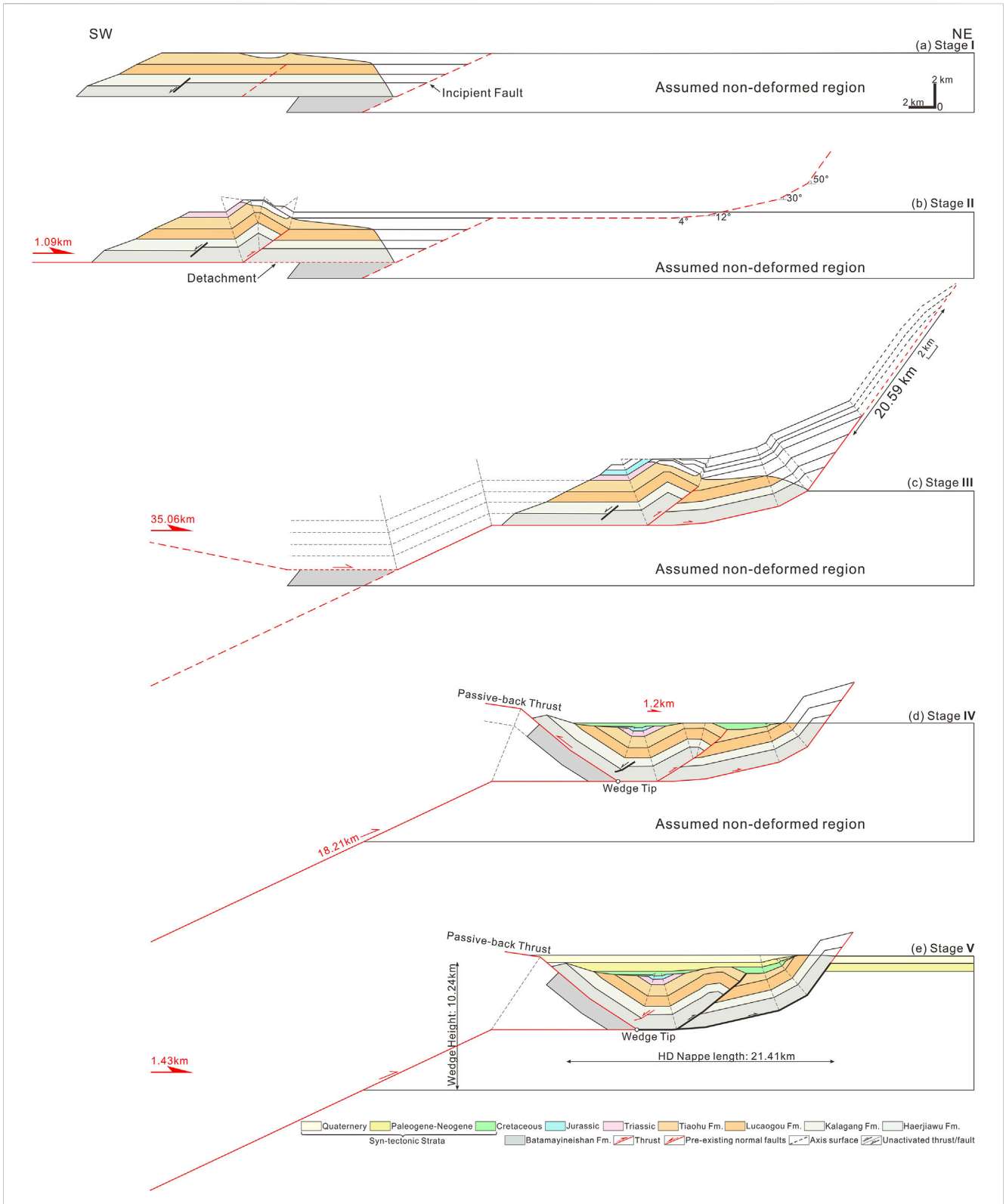

FIGURE 10
Schematic forward model of the Heidrun thrust nappe in the southwestern Santanghu Basin. **(A)** Stage I: undeformed state of the Heidrun thrust nappe. **(B)** Stage II: initiation of the fault-propagation fold related to the Haerjiawu Formation detachment. **(C)** Stage III: the Heidrun thrust nappe system forms a fault-bend fold during the broadening period along the thrust ramp and flat. **(D)** Stage IV: initiation of the basement structural wedge. **(E)** Stage V: the structural wedge tip breaks forward, which shows synchronous slipping of the lower and upper ramp thrust along the Haerjiawu Formation detachment.

established a reasonable evolution model to explain the influence of the differential activity of the internal faults of the nappe on the structure of the pre-growth strata and the syntectonic sedimentary strata (Figure 10). In the initial stage of compression, the Baiyishan branch fault F1 ruptured along the pre-setting Haerjiawu Formation detachment layer, with a shortening displacement of 1.09 km, forming a breakthrough fault-propagation fold (Figures 10A, B). An upper thrust ramp with a dip angle of approximately 25° was set up approximately 12 km ahead of the F2 fault syncline hinge, and four sets of multi-step ramp faults in the dip angle domain were set up at the front end of the hanging wall falt. During the 35.06 km compression shortening process preset in stage 2, the strata on the hanging wall of the fault slide along the flat and ramp of the F2 fault entered into the fold crestal broadening period of the fault-bend fold (Figure 10C). During this process, approximately 0.75 km of displacement was assigned to the F1 fault. As the syntectonic growth strata were consistent with the ramp and flat structure of the F2 fault, it indicated that the F1 fault did not participate in deformation. Therefore, the roof detachment layer of the structural wedge developed along the basement was the Haerjiawu Formation. Along the pre-existing Baiyishan fault ramp, 18.21 km was wedged, of which 1.2 km displacement belonged to the forward breakthrough of the wedge endpoint, and the growth triangle zone was developed in the front edge of the syntectonic sedimentary strata (Figure 10D). In the final period, the wedge endpoint continued to break through 1.43 km forward, and the deposition rate was higher than the fault slip rate to ensure that the strata overlap unconformably on the paleotopography. The simulation results show that the Heidrun nappe is approximately 21.41 km wide, the tectonic uplift reaches 10.24 km, and the vertical and lateral amplitudes are 2 km more than the actual value (Figure 10E; Figure 7). This may be attributed to the fact that our forward model only simulates the kinematics of the faults inside the nappe and make ideal assumptions about the shape of the basement. There is no flexural load effect of the piedmont basin caused by the orogenic movement. Previous studies have shown that the structure of the piggy-back basin is controlled by the mutual regulation of regional basement subsidence and local thrust deformation and erosion activities (Ori and Friend, 1984; Decelles and Giles, 1996; Chanvry et al., 2018; Chen and He, 2022). However, the adjustment of multiple factors provides greater difficulties for forward modeling, which is beyond the scope of this study.

5.2 Implication for the Yanshanian–Himalayan intracontinental deformation of Moqinwula Mountain

The formation of the Heidrun nappe is a typical model for the development of the piggy-back basin. The activity scale and sequence combination of its internal faults provide a good case for studying the intracontinental deformation mechanism of orogenic activation from Yanshanian to Himalayan in the Eastern Tianshan tectonic domain.

After the denudation and planation in the Indosinian movement, the entire Xinjiang region was in a quasi-plain landscape in the Early–Middle Jurassic (Zhao et al., 2020). The Jurassic coal measure strata distributed in the higher parts of the Tianshan region, which could witness the existence of this paleogeographic environment (e.g., Zhang et al., 2013; Yang et al., 2015; Zhang et al., 2022). In the late Middle Jurassic–Late Jurassic, controlled by the closure of the Okhotsk Ocean (Cogné et al., 2005; Zhang et al., 2019) and the remote effect of the Late Jurassic–Early Cretaceous scissor-type closure of the Bangong–Nujiang Ocean from east to west, the northern part of Xinjiang is generally in a tectonic environment of transpression deformation (Ma et al., 2017; Peng et al., 2020). A field study of the Jurassic folds and faults in the Moqinwula Mountains by Chen et al., 2020a suggested that the regional tectonic stress field changed from NE-SW compression to N-S compression after the Early Jurassic, and the radial thrusting of the southern-northern orogenic belt in the Santanghu Basin became stronger. The restoration results of the nappes in the southwestern margin of the basin show that during this period, the basin margin was compressed to form a long-distance nappe structure along the Carboniferous detachment layer, with a horizontal shortening distance of at least 35 km (Figure 9). In addition, the Xixiagou anticline in the northern part of the basin also exposed a large area of the Lower Cretaceous and Jurassic unconformities on the surface (Figure 2). This is consistent with the apatite fission age obtained by other scholars in Moqinwula Mountain, and the thermal history simulation results also reveal the cooling process of the rapid uplift of the Late Jurassic–Late Cretaceous (Gillespie et al., 2017; Chen et al., 2020b).

In the Early Cretaceous, the rapid cooling event was generally recorded in the Tianshan area due to the southward closure of the Middle Tethys Ocean and the initial collision event between the Lhasa terrane and the southern margin of Asia in Tibet (Gillespie et al., 2017; Kapp and Decelles, 2019; He et al., 2022). In contrast, the compression of the S-N orogenic belt in the Santanghu Basin was weak, and the subsidence of the southwest margin piggy-back basin accepted the deposition of the Lower Cretaceous (Figure 6). In addition, the fluvial–shallow lacustrine sedimentary system was widely developed in the basin, indicating that the orogenic activity in the periphery was not strong at that time (Figures 3, 4). In the Late Cretaceous–Paleogene, the compression of the southern and northern fold–thrust belt of the Santanghu Basin was gradually strengthened by the remote influence of the Lhasa–Qiangtang collision (120–90 Ma) and the Kohistan–Dras arc collision event (Yin and Harrison, 2000; Rehman et al., 2011; Chen et al., 2020a). The southern margin fold–thrust belt is mainly dominated by the activation of pre-existing thrust faults. Fold thrust and uplift caused the Cretaceous in the basin to be eroded, forming a regional unconformity between the Cretaceous and Paleogene. Overlapping and truncation unconformities are developed in the uplift belt or basin margin belt, and the depression area is in parallel unconformities (Figure 8).

In the Late Cenozoic, due to the remote effect of the collision between the Eurasian continent and the Indian plate, the Tianshan region entered a rapid cooling stage (Tapponnier and Molnar, 1979; De Grave et al., 2007; Charreau et al., 2009). However, the related thermal history simulation studies suggest that the uplift of Moqinwula Mountain in the northern part of Eastern Tianshan is relatively limited (Gillespie et al., 2017). In particular, the thermal history of tectonic evolution in southern Moqinwula Mountain indicates that the Paleogene–Quaternary

experienced a slow cooling process, with an average temperature decrease of 20°C–25°C (Chen et al., 2020b). Our structural model also reveals that the reactivation of basement faults in the basin margin caused the forced folds of the Quaternary in the piedmont zone, while the Quaternary in the basin is a wedge-shaped basin tilted southward, with no obvious tectonic deformation record (Figure 6).

6 Conclusion

In this paper, based on the high-resolution seismic profiles and electromagnetic profiles, the Heidrun thrust nappe in the fold–thrust belt on the southwestern margin of the Santanghu Basin develops the thrust faults and back-thrust faults that cut the Devonian–Carboniferous to form a structural wedge. The detachment layer of the Carboniferous Haerjiawu Formation develops two branch faults to the north, forming a relatively intact breakthrough fault-propagation fold and fault-bend fold. The growth strata and unconformity structure record that the fold–thrust belt experienced five episodes of episodic thrusting from the Late Triassic to Quaternary. Based on sequential restoration and forward modeling, we propose that the fold–thrust belt in the southwestern margin of the Santanghu Basin has been shortened by at least 55 km. Our study provides an episodic thrust evolution model of the Heidrun thrust nappe in the Late Jurassic–Quaternary and provides a good case for studying the intracontinental deformation mechanism of orogenic activation from Yanshanian transpression to Himalayan thrust compression in the Eastern Tianshan tectonic domain.

Data availability statement

The original contributions presented in the study are included in the article/Supplementary Material; further inquiries can be directed to the corresponding author.

Author contributions

YZ: investigation, conceptualization, methodology, software, and writing–original draft. XX: data curation, supervision, visualization, and writing–review and editing. DH: supervision, writing–review and editing, funding acquisition, and project administration. XL: supervision, writing–review and editing, and data curation. DL: supervision, writing–review and editing, and investigation.

Funding

The authors declare financial support was received for the research, authorship, and/or publication of this article. This research was financially supported by the National Natural Science Foundation of China (42172124 and U19B6003), the joint project of PetroChina: Research on Carboniferous Petroleum Geological Conditions and Exploration Direction Selection in Tuha Exploration Area (2021DJ0306), and Research on Marine Devonian and Carboniferous Petroleum Geology in Northern Xinjiang (2022DJ0507).

Acknowledgments

The authors thank the Tuha Oilfield of China National Petroleum Corporation for providing the electromagnetic profile, the seismic reflection profile, and drilling data.

Conflict of interest

The authors declare that this study received funding from the joint project of PetroChina: Research on Carboniferous Petroleum Geological Conditions and Exploration Direction Selection in Tuha Exploration Area (2021DJ0306). The funder had the following involvement in the study: the study design, collection, analysis, interpretation of data, the writing of this article, and the decision to submit it for publication.

XX and XL were employed by Tuha Oilfield Company, PetroChina.

The remaining authors declare that the research was conducted in the absence of any commercial or financial relationships that could be construed as a potential conflict of interest.

Publisher's note

References

Alania, V. M., Chabukiani, A. O., Chagelishvili, R. L., Enukidze, O. V., Tsereteli, N. S., Razmadze, A. N., et al. (2017). Growth structures, piggy-back basins and growth strata of the Georgian part of the kura foreland fold–thrust belt: implications for late alpine kinematic evolution. *Geol. Soc. Lond. Spec. Publ.* 428 (1), 171–185. doi:10.1144/sp428.5

Alania, V., Melikadze, G., Pace, P., Fórizs, I., Beridze, T., Enukidze, O., et al. (2022). Deformation structural style of the rioni foreland fold- and-thrust belt, western greater caucasus: insight from the balanced cross-section. *Front. Earth Sci.* 10, 968386. doi:10.3389/feart.2022.968386

Allen, P. A., and Allen, J. R. (2013). *Basin analysis: Principles and application to Petroleum play assessment*. John Wiley & Sons.

Bureau of Geology and Mineral Resoures of Xinjiang Uygur Autonomous Region (BGMRXUAR) (1966). *Geological maps of Santanghu area (scale 1:200,000)*. Xinjiang Bureau of Geology and Mineral Resources.

Chanvry, E., Deschamps, R., Joseph, P., Puigdefàbregas, C., Poyatos-Moré, M., Serra-Kiel, J., et al. (2018). The influence of intrabasinal tectonics in the stratigraphic evolution of piggyback basin fills: towards a model from the tremp-graus-ainsa basin (South-Pyrenean zone, Spain). *Sediment. Geol.* 377, 34–62. doi:10.1016/j.sedgeo.2018.09.007

Charreau, J., Gumiaux, C., Avouac, J. P., Augier, R., Chen, Y., Barrier, L., et al. (2009). The Neogene xiyu formation, adiachronous prograding gravel wedge at front of the tianshan: climatic and tectonic implications. *Earth Planet. Sci. Lett.* 287, 298–310. doi:10.1016/j.epsl.2009.07.035

Charvet, J., Shu, L. S., and Laurent-Charvet, S. (2007). Paleozoic structural and geodynamic evolution of eastern Tianshan (NW China): Welding of the Tarim and Junggar plates. *Episodes* 30 (3), 162–186.

Chen, J. J., and He, D. F. (2022). Geometry, kinematics and mechanism of growth unconformities in the biertuokuoyi piggy-back basin: implications for episodic growth of the pamir frontal thrust. *J. Geol. Soc.* 179. doi:10.1144/jgs2021-100

Chen, S., Zhang, Y. Y., and Guo, Z. J. (2009). Zircon SHRIMP U-Pb dating and its implications of post-collisional volcanic rocks in Santanghu Basin, Xinjiang. *Acta Petrol. Sin.* 25 (3), 527–538.

Chen, Y., Wang, G. C., Kapp, P., Shen, T. Y., Zhang, P., Zhu, C. Y., et al. (2020a). Episodic exhumation and related tectonic controlling during Mesozoic in the Eastern Tian Shan, Xinjiang, northwestern China. *Tectonophysics* 796, 228647. doi:10.1016/j.tecto.2020.228647

Chen, Y., Wang, G., Shen, T., Zhang, P., Sotirious, P., and Zhu, C. (2020b). Tectono-geomorphic evolution of Harlik Mountain in the Eastern Tian Shan, insight from thermochronological data and geomorphic analysis. *Geol. J.* 55, 7322–7334. doi:10.1002/gj.3951

Cogné, J. P., Kravchinsky, V. A., Halim, N., and Hankard, F. (2005). Late Jurassic-early cretaceous closure of the Mongol-Okhotsk Ocean demonstrated by new Mesozoic palaeomagnetic results from the Trans-Baïkal area (SE Siberia). *Geophys. J. Int.* 163 (2), 813–832. doi:10.1111/j.1365-246x.2005.02782.x

Davis, D., Suppe, J., and Dahlen, F. (1983). Mechanics of fold-and-thrust belts and accretionary wedges. *J. Geophys. Res. Solid Earth* 88, 1153–1172. doi:10.1029/jb088ib02p01153

De Grave, J., Buslov, M. M., and Van den Haute, P. (2007). Distant effects of India-eurasia convergence and mesozoic intracontinental deformation in central Asia: constraints from apatite fission track thermochronology. *J. Asian Earth Sci.* 29, 188–204. doi:10.1016/j.jseaes.2006.03.001

DeCelles, P. G., and Giles, K. A. (1996). Foreland basin systems. *Basin Res.* 8, 105–123. doi:10.1046/j.1365-2117.1996.01491.x

DeCelles, P. G. (2011). "Foreland basin systems revisited: variations in response to tectonic settings," in *Tectonics of sedimentary basins: Recent advances*, 405–426. doi:10.1002/9781444347166.ch20

Gillespie, J., Glorie, S., Jepson, G., Zhang, Z. Y., Xiao, W. J., Danisík, M., et al. (2017). Differential exhumation and crustal tilting in the Easternmost Tianshan (Xinjiang, China), revealed by low-temperature thermochronology. *Tectonics* 36 (10), 2142–2158. doi:10.1002/2017tc004574

He, Z. Y., Wang, B., Glorie, S., Su, W. B., Ni, X. H., Jepson, G., et al. (2022). Mesozoic building of the eastern tianshan and East Junggar (NW China) revealed by low-temperature thermochronology. *Gondwana Res.* 103, 37–53. doi:10.1016/j.gr.2021.11.013

Huang, B., Dong, F., Kusky, T., Ruan, K. P., Zhou, W.,X., and Zhang, X. H. (2018). Sedimentary provenance in response to carboniferous arc-basin evolution of East Junggar and north tianshan belts in the southwestern central asian orogenic belt. *Tectonophysics* 722, 324–341. doi:10.1016/j.tecto.2017.11.015

Izquierdo-Llavall, E., Roca, E., Xie, H., Pla, O., Muñoz, J. A., Rowan, M. G., et al. (2018). Influence of overlapping décollements, syntectonic sedimentation, and structural inheritance in the evolution of a contractional system: the central kuqa fold-and-thrust belt (tian Shan mountains, NW China). *Tectonics* 37, 2608–2632. doi:10.1029/2017TC004928

Jiang, X. D., and Li, Z. X. (2014). Seismic reflection data support episodic and simultaneous growth of the Tibetan Plateau since 25 Myr. *Nat. Commun.* 5, 5453. doi:10.1038/ncomms6453

Jolivet, M., Heilbronn, G., Robin, C., Barrier, L., Bourquin, S., Guo, Z., et al. (2013). Reconstructing the late palaeozoic-mesozoic topographic evolution of the Chinese tian Shan: available data and remaining uncertainties. *Adv. Geosciences* 37, 7–18. doi:10.5194/adgeo-37-7-2013

Kapp, P., and Decelles, P. G. (2019). Mesozoic-Cenozoic geological evolution of the Himalayan-Tibetan orogen and working tectonic hypotheses. *Am. J. Sci.* 319, 159–254. doi:10.2475/03.2019.01

Li, D., He, D. F., Sun, M., and Zhang, L. (2020). The role of arc-arc collision in accretionary orogenesis: insights from ~320 Ma tectono-sedimentary transition in the karamaili area, NW China. *Tectonics* 39. doi:10.1029/2019tc005623

Lu, H. O., Yuan, B. Q., Li, Y. H., Zhang, C. G., and Shen, C. (2012). Characteristics of fault structures in Santanghu Basin. *Xinjiang Pet. Geol.* 33 (3), 4.

Ma, R. S., Wang, C. Y., and Ye, S. F. (1993). *Tectonic framework and crustal evolution of eastern Tianshan mountains*. Nanjing: Publication House of Nanjing University, 1–225.

Ma, A., Hu, X., Garzanti, E., Han, Z., and Lai, W. (2017). Sedimentary and tectonic evolution of the southern qiangtang basin: implications for the lhasa-qiangtang collision timing. *J. Geophys. Res. Solid Earth* 122, 4790–4813. doi:10.1002/2017jb014211

Ori, G. G., and Friend, P. F. (1984). Sedimentary basins formed and carried piggyback on active thrust sheets. *Geology* 12 (8), 475–478. doi:10.1130/0091-7613(1984)12<475:sbfacp>2.0.co;2

Peng, Y. B., Yu, S. Y., Li, S. Z., Liu, Y. J., Santosh, M., Lv, P., et al. (2020). The odyssey of Tibetan plateau accretion prior to cenozoic India-Asia collision: probing the mesozoic tectonic evolution of the bangong-nujiang suture. *Earth Sci. Rev.* 211, 103376. doi:10.1016/j.earscirev.2020.103376

Rehman, H. U., Seno, T., Yamamoto, H., and Khan, T. (2011). Timing of collision of the kohistan-ladakh arc with India and Asia: debate. *Isl. Arc* 20 (3), 308–328. doi:10.1111/j.1440-1738.2011.00774.x

Sengör, A. M. C., Natal'in, B. A., and Burtman, V. S. (1993). Evolution of the Altaid tectonic collage and Palaeozoic crustal growth in Eurasia. *Nature* 364 (6435), 299–307. doi:10.1038/364299a0

Shu, L. S., Lu, H. F., Yin, D. H., Ma, R. S., Xia, F., and Lu, H. (2001). Late Paleozoic continental accretionary tectonics in northern Xinjiang. *Xinjiang Geol.* 19 (1), 59–63. doi:10.3969/j.issn.1000-8845.2001.01.011

Si, X. Q., Guo, M. Z., Yang, Z. L., Chen, X., Wang, X., and Cao, Q. B. (2015). Sedimentary characteristics and models of the Jurassic Xishanyao Formation in Malang Depression, Santanghu Basin, Xinjiang. *J. Palaeogeogr.* 17 (004), 553–564. doi:10.7605/gdlxb.2015.04.045

Sun, J., and Zhang, Z. (2009). Syntectonic growth strata and implications for late Cenozoic tectonic uplift in the northern Tian Shan, China. *Tectonophysics* 463, 60–68. doi:10.1016/j.tecto.2008.09.008

Sun, Z. M., Xiong, B. X., Li, Y. L., and He, H. Q. (2001). Structural characteristic and favorable belt of fracture exploration in Santanghu Basin. *Petroleum Geol. Exp.* 23 (1), 23–26. doi:10.11781/sysydz200101023

Suppe, J., and Medwedeff, D. A. (1990). Geometry and kinematics of fault-propagation folding. *Eclogae Geol. Helvetiae* 83, 409–454.

Tapponnier, P., and Molnar, P. (1979). Active faulting and cenozoic tectonics of the tien Shan, Mongolia, and baykal regions. *J. Geophys. Res.* 84, 3425–3459. doi:10.1029/jb084ib07p03425

Tesón, E., and Teixell, A. (2008). Sequence of thrusting and syntectonic sedimentation in the eastern Sub-Atlas thrust belt (Dadès and Mgoun valleys, Morocco). *Int. J. Earth Sci.* 97, 103–113. doi:10.1007/s00531-006-0151-1

Tesón, E., Teixell, A., and Arboleya, M. L. (2010). Intraplate tectonics: insights from mountain building in the Moroccan atlas and related subsidence in the ouarzazate foreland basin. *Trab. Geol.* 301, 266–272.

Wang, G. C., Zhang, M., Zhang, X. H., Liao, Q. A., Wang, W., Tian, J. M., et al. (2019). Significant Paleozoic tectonic events in the northern part of the East Tianshan Mountains, Xinjiang and their implications for the evolution of CAOB: New evidence from 1: 50000 geological survey of Banfanggou and Xiaoliugou sheets. *Geol. China* 46 (5), 954–976. doi:10.12029/gc20190502

Windley, B. F., Alexeiev, D. V., Xiao, W., Kröner, A., and Badarch, G. (2007). Tectonic models for accretion of the central asian orogenic belt. *J. Geol. Soc.* 164, 31–47. doi:10.1144/0016-76492006-022

Wu, X. Z., Lang, F. J., Li, B. H., Qi, X. F., and Liu, D. G. (2011). Structure evolution and petroleum accumulation of Santanghu Basin. *Chin. J. Geol.* 46 (3), 808–825.

Xiao, W. J., Zhang, L. G., Qin, K. Z., Sun, S., and Li, J. L. (2004). Paleozoic accretionary and collisional tectonics of the eastern tianshan (China): implications for the continental growth of central Asia. *Am. J. Sci.* 304, 370–395. doi:10.2475/ajs.304.4.370

Xiao, W. J., Windley, B. F., Yuan, C., Sun, M., Han, C. M., Lin, S. F., et al. (2009). Paleozoic multiple subduction-accretion processes of the southern Altaids. *Am. J. Sci.* 309, 221–270. doi:10.2475/03.2009.02

Yang, Y. T., Song, C. C., and He, S. (2015). Jurassic tectonostratigraphic evolution of the junggar basin, NW China: a record of mesozoic intraplate deformation in central Asia. *Tectonics* 34, 86–115. doi:10.1002/2014tc003640

Yin, A., and Harrison, T. M. (2000). Geologic evolution of the Himalayan-Tibetan orogen. *Annu. Rev. Earth Planet. Sci.* 28, 211–280. doi:10.1146/annurev.earth.28.1.211

Yu, W., Shao, Z. G., Niu, M. L., Su, H., Zhang, Y. P., and Wang, Y. C. (2023). Intracontinental evolution of the southern central asian orogenic belt: evidence from late triassic nappe structure in the northern alxa region, NW China. *J. Asian Earth Sci.* 243, 105468–109120. doi:10.1016/j.jseaes.2022.105468

Zhang, H., Kuang, H. W., Liu, Y. Q., and Peng, N. (2013). Th1/Th2/Th17/Treg cytokines in Guillain-Barré syndrome and experimental autoimmune neuritis. *Geol. Bull. China* 32 (2/3), 443–453. doi:10.1016/j.cytogfr.2013.05.005

Zhang, H. H., Zhang, Z. C., Tang, W. H., Li, K., Li, J. F., Wang, Q., et al. (2022). Burial and exhumation history of Jurassic sedimentary rocks in the southern margin of the Junggar Basin: Implications for the growth of the northern Tianshan Mountains. *J. Asian Earth Sci.* 236, 105339. doi:10.1016/j.jseaes.2022.105339

Zhang, Y. Q., Dong, S. W., Meng, Y., Zhao, Y. N., and Liu, D. G. (2019). Morphologic analysis of maxillary sinus floor and its correlation to molar roots using cone beam computed tomography. *J. Geomechanics* 25 (5), 29–36. doi:10.3290/j.cjdr.a41772

Zhao, R., Zhang, J. Y., Zhou, C. M., Zhang, Z. J., Chen, S., Stockli, D. F., et al. (2020). Tectonic evolution of Tianshan-Bogda-Kelameili mountains, clastic wedge basin infill and chronostratigraphic divisions in the source-to-sink systems of Permian-Jurassic, southern Junggar Basin. *Mar. Petroleum Geol.* 114, 104200. doi:10.1016/j.marpetgeo.2019.104200

Zhou, M. F., Lesher, C. M., Yang, Z. X., Li, J. W., and Sun, M. (2004). Geochemistry and petrogenesis of 270 Ma Ni–Cu–(PGE) sulfide-bearing mafic intrusions in the huangshan district, eastern Xinjiang, northwest China: implications for the tectonic evolution of the central asian orogenic belt. *Chem. Geol.* 209, 233–257. doi:10.1016/j.chemgeo.2004.05.005